We are IntechOpen, the world's leading publisher of Open Access books Built by scientists, for scientists

6,900
Open access books available

185,000
International authors and editors

200M
Downloads

Our authors are among the

154
Countries delivered to

TOP 1%
most cited scientists

12.2%
Contributors from top 500 universities



WEB OF SCIENCE™

Selection of our books indexed in the Book Citation Index in Web of Science™ Core Collection (BKCI)

Interested in publishing with us?
Contact book.department@intechopen.com

Numbers displayed above are based on latest data collected.
For more information visit www.intechopen.com



17

A New Rapid Prototyping Process for Sheet Metal Parts

Luo, Yuanxin[1], He, Kai[2] and Du, Ruxu[3]
[1]*Chongqing University*
[2]*Shenzhen Institute of Advanced Technology*
[3]*The Chinese University of Hong Kong*
[3]*Hong Kong*
[1,2]*China*

1. Introduction

In recent years, various kinds of dieless sheet metal forming methods are developed. As it does not use dies, dieless sheet metal forming, also called Incremental Sheet Metal Forming (ISMF), is effective for small batch production and prototypes. Today, it has become one of the leading R&D topics in the industry.

Based on literature review, a number of ISMF methods have been developed. Nakajima first proposed the concept of flexible computer controlled forming process and anticipated the development of incremental forming (Nakajima, 1979). In subsequent years, a number of significant developments followed. Mori and Yamamoto proposed a new incremental forming method, in which the forming was carried out by a series of movements using a hemispherical hammer hammering the metal sheet into a 3D shape (Mori, et al., 1996). A simple hemispherical part was made. Saotome and Okamoto designed an incremental microforming system to for 3D shell structure (Saotome & Okamoto, 2001). Schafer and Schaft conducted experiments using an industrial robot (Schafer & Schraft, 2005). Callegari et al. (2008) used a parallel kinematics machines to carry on an ISMF experiment. Amino and Ro (2001) designed and built a CNC controlled ISMF system. The workpiece was held by a moving table under the press of a rotating forming tool. This method is also studied by Kopac and Campus (2005), Kim and Park (2003), Ceretti et al. (2004), Micari et al. (2007), Ham and Jeswiet (2007), Silva et al. (2009) and Ambrogio et al. (2009). Allwood et al. (2009) designed a close-loop system by integrated a vision system into the CNC ISMF system. Callegari et al. (2007) compared the advantages of ISMF forming method by using robot cells and CNC machines. It should be noted that most of these experiments are based either on a CNC machine with a rotating tool (see Figure 1), or a robot with hammer (see Figure 2).

Despite of some 30 years of research and development, ISMF technology is still premature for industrial applications due to the following reasons. (a) The accuracy of the part is limited (usually less than 1 mm); (b) the heat generated due to the continuous contact between the material and the forming tool is significant and hence, lubrication is indispensable; (c) the surface roughness is poor; and (d) the productivity is low.

This chapter introduces a new ISMF system. It uses a high frequency punch hammer controlled by a CNC machine (Luo et al., 2010a, 2010b). It forms a part punch by punch and

layer by layer. It should be point out that such an incremental punching method can be divided into two kinds: one is without the bottom support and the other is with the bottom support, as illustrated in Figure 3(a) and 3(b) respectively. The former is simpler, but the later would give better accuracy and could make more complex parts.

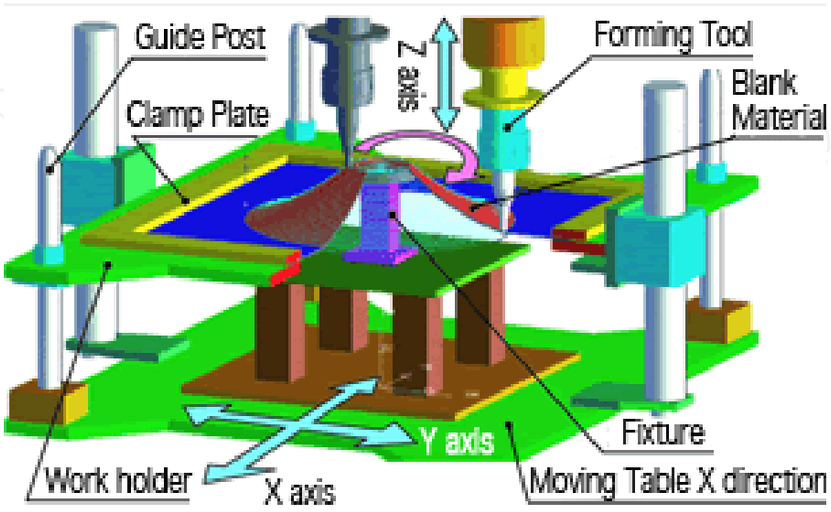
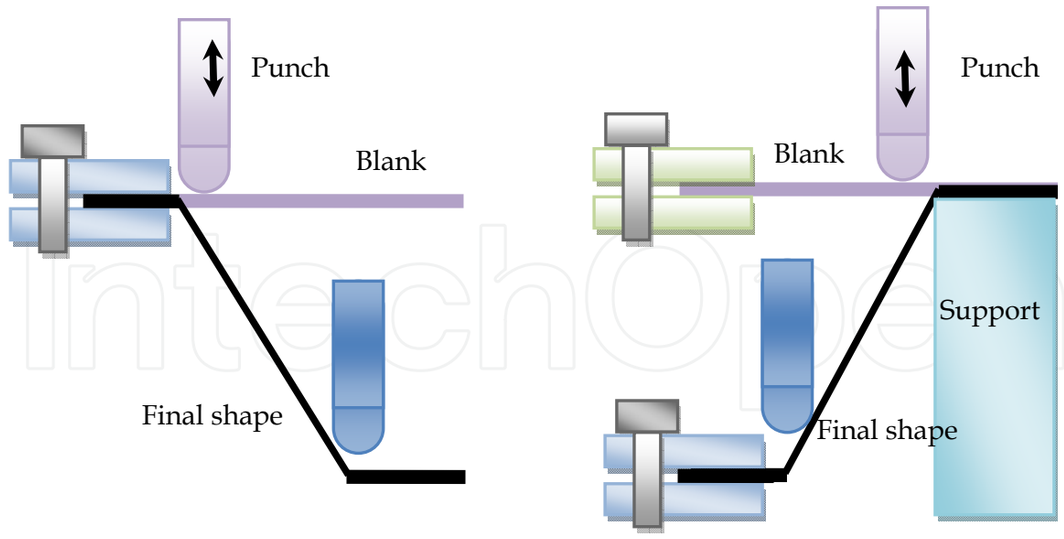


Fig. 1. Illustration of a CNC ISMF system (Amino Co., 2006)



Fig. 2. A robot based ISMF system (Schafer et al, 2005)

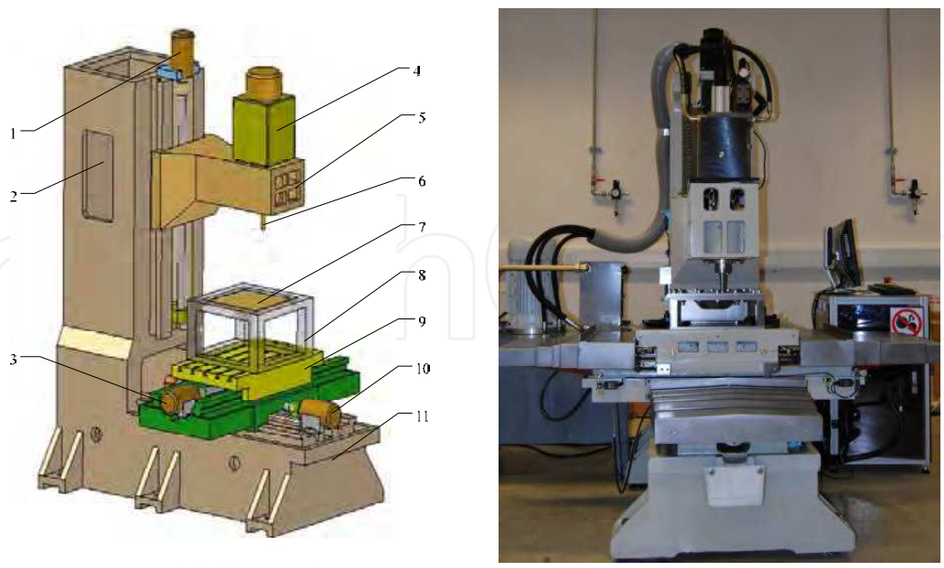


(a) without support (b) with support

Fig. 3. Illustrations of incremental punching methods

2. Design and building of the ISMF machine

We designed and built a new ISMF machine as shown in Figure 4. The machine was built based on a standard CNC machine. Mechanically, it consists of four components: a X-Y table, a Z slider, a fixture, and a high speed hydraulic punch. The X-Y table is driven by two servomotors. The workpiece is clamped by the fixture mounted on the X-Y table. The slider



(a) illustration (b) photo

Fig. 4. Our ISMF machine, 1 – Z axis servomotor and encoder, 2 – Balancing weight, 3 – X axis servomotor and encoder, 4 – High speed punch head, 5 – Z Slider, 6 – Forming tool, 7 – Workpiece, 8 – Fixture, 9 – X-Y table, 10 – Y axis servomotor and encoder, 11 – Frame.

moves in Z direction with the hydraulic punch head mounted on the top. To balance the gravity force of the slider and the hydraulic punch head, a balancing weight is used. The work volume of the machine is 500 mm × 500 mm × 600 mm.
The machine is controlled by an industrial PC computer. Figure 5 shows the control structure. The X-Y table and the Z slider are controlled by a motion control card. After tuning the PID parameters, their position accuracies are about 0.01 mm.

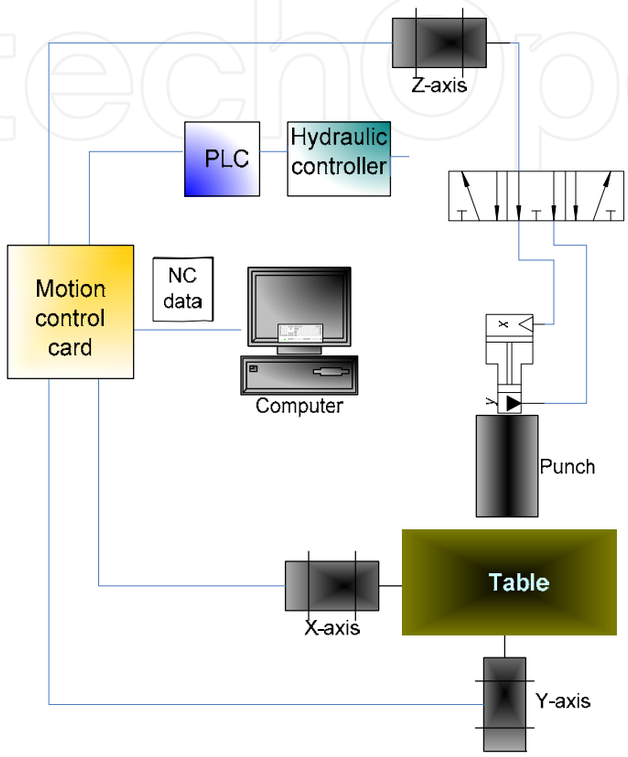


Fig. 5. The control system of our ISMF machine

The high speed hydraulic system is a key component (manufacturer: Voith Turbo H + L Hydraulic; model: ECO 20), it can provide 10 tons force and has a maximum speed of 300 Strokes Per Minute (SPM) when the stroke is within 5 mm. It has its own closed-loop control system that can communicate with the PC computer.
The machine uses a simple fixture, or blank holder. The square workpiece is simply mounted on the fixture along the edges and there is no additional support. As shown in Figure 6, in the experiments, two different configurations are used: L = 220 mm (Setup A), and L = 260 mm (Setup B).
To facilitate the operation, four different ball-end punch heads are made, as shown in Figure 7. Their diameters are 5 mm, 10 mm, 15mm, and 20 mm respectively. The size of the ball end punch head determines not only the minimum curvature of the part but also the surface roughness of the part. It also affects the punch force.

3. The punch path generation

The operation of the new ISMF is in fact rather similar to that of an experienced smith. The workpiece is mounted on the fixture. Along the depth of the part, the part is divided into a

number of layers. At each layer, from the top to the bottom, the workpiece is punched step by step along the contour of the layer. When one layer is done, the Z slider moves down. The whole operation is finished when the all the layers are done. Clearly, the shape and the accuracy of the part are largely determined by the punch locations, and the collection of the punch locations will be referred to as the punch path.

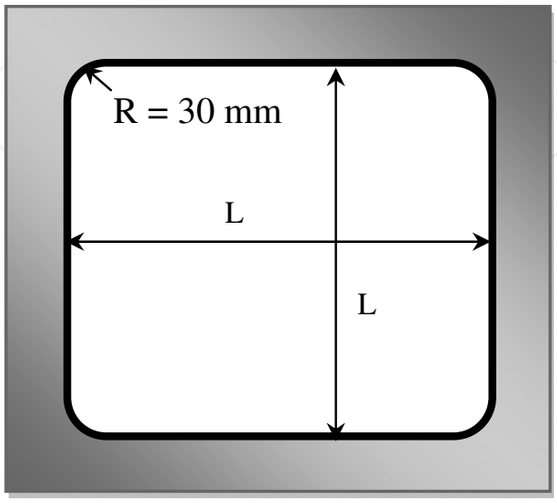
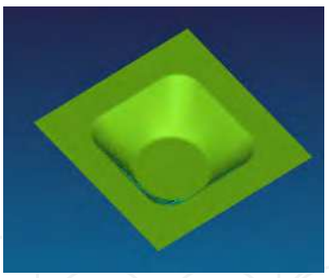


Fig. 6. Illustration of the fixture size

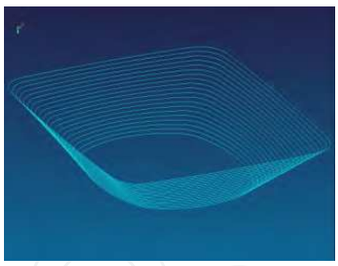


Fig. 7. The ball-end punch heads

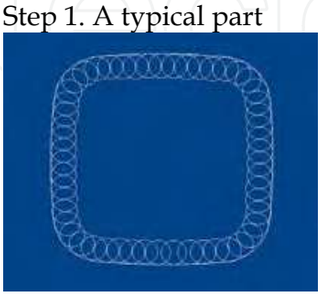
The punch path is similar to the cutter path in CNC machining. As illustrated in Figure 8, to generate the punch path, the part is first sliced into a number of layers. For each layer, next, the contour of the part is found. Then, the punch path is generated based on the geometry of the contour. This can be done using commercial software systems, such as MasterCAM®. Finally, the punch paths for different layers are stitched to form the complete punch path.



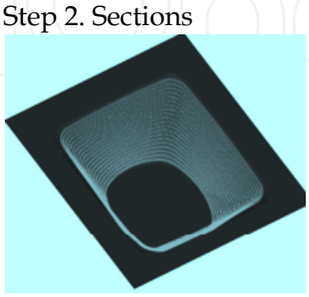
Step 1. A typical part



Step 2. Sections



Step 3. A contour



Step 4. Punch locations

Fig. 8. The punch path generation process

During the punch path generation, the feed of the punch is important. The layer thickness, h, is the feed in the Z axis (the vertical direction feed). The feed rate in the XY direction (the horizontal direction feed) is calculated based on the following equation:

$$F = \frac{a \times f}{60} (\text{mm} / \text{min}) \tag{1}$$

where, a is the feed step size (mm) and f is the punch speed (SPM).
Given the layer thickness, h, and the feed step size a, the resulting geometric error can be

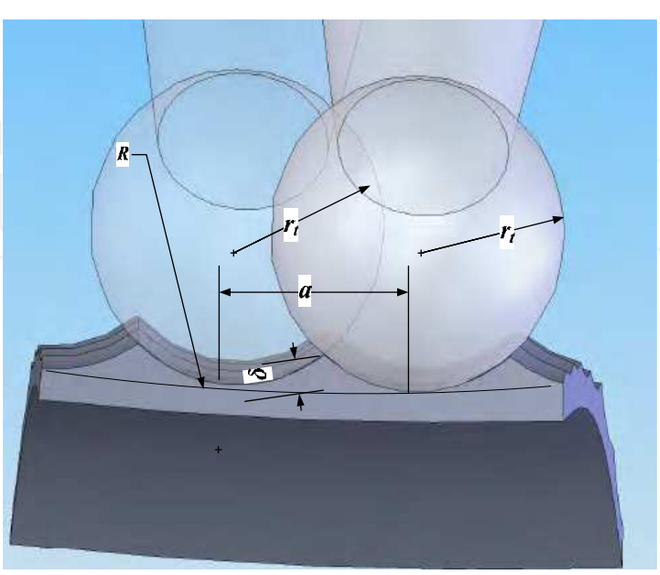


Fig. 9. Illustration of the geometric error on a surface contour

found. Figure 9 illustrates the geometric relationship of a part contour along the horizontal direction, and the ball-end punch. It can be shown that the geometric error, δ, is as follows:

$$\delta = \begin{cases} r_t - \sqrt{r_t^2 - \dfrac{a^2}{4}} & R = 0 \\ R - \sqrt{(r_t - R)^2 - \dfrac{a^2}{4}} - \sqrt{r_t^2 - \dfrac{a^2}{4}} & R > 0 \\ \sqrt{(r_t - R)^2 - \dfrac{a^2}{4}} - \sqrt{r_t^2 - \dfrac{a^2}{4}} + R & R < 0 \end{cases} \tag{2}$$

where, rt is the radius of the ball-end punch head, and R is the curvature of the part contour. Hence, given the maximum geometric tolerance, δmax, the maximum feed step size can be defined as follows:

$$a = \frac{\sqrt{s \cdot (s - r_t)(s - R + r_t)(s - R + \delta_{\max})}}{2(R - \delta_{\max})} \tag{3}$$

Similarly, along the vertical direction, the geometric error can be found from the geometric relationship as shown in Figure 10. It is as follows:

$$\delta = \begin{cases} r_t - \sqrt{r_t^2 - \dfrac{h^2}{4}} & R' = 0 \\ R' - \sqrt{(r_t - R')^2 - \dfrac{h^2}{4}} - \sqrt{r_t^2 - \dfrac{h^2}{4}} & R' > 0 \\ \sqrt{(r_t - R')^2 - \dfrac{h^2}{4}} - \sqrt{r_t^2 - \dfrac{h^2}{4}} + R' & R' < 0 \end{cases} \tag{4}$$

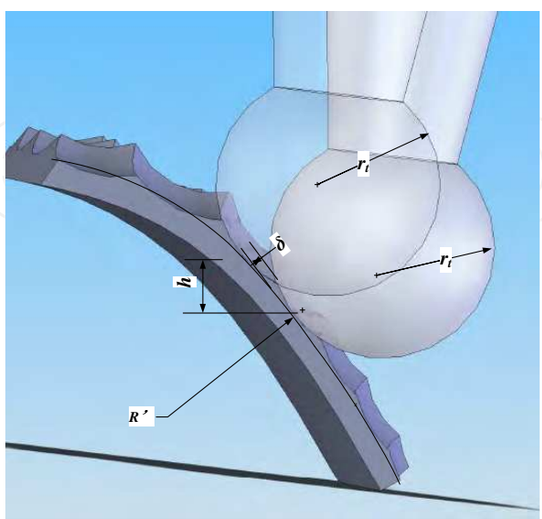


Fig. 10. The geometric error in vertical cross section

where, R′ is the radius of curvature in the cross section plane. Given the maximum geometric tolerance, δmax, the maximum thickness of the layer will,

$$h = \frac{\sqrt{s \cdot (s - r_t)(s - R' + r_t)(s - R' + \delta_{\max})}}{2(R' - \sigma_{\max})} \tag{5}$$

where, $s = R' - \frac{\delta_{\max}}{2}$.

As mentioned earlier, when the feeds are decided, the punch path can be generated using commercial CAM software systems, such as MasterCAM®. It takes only a few minutes. The surface finish can also be estimated.

4. Mechanics model of incremental punching

In the old days, trial and error method was always used to improve the design of dies in conventional stamping. Tuomi and Lamminen (2004) presented a general production process of ISMF that can be utilized for most of existing ISMF process. However, the quality improvement will be depended on experience of the worker.

It's reported that the commercial FEM packages can be used to simulate the forming process instead of trial-and-error method. A modified process is proposed for the whole forming process, which is shown in Figure 11. In this process, firstly, a CAD model is build based on the conception of desired part. Secondly, the initial tool path is generated in the CAM software according to the geometric relations. Thirdly, FEA simulation is conducted to predict the final shape and the strain / stress distributions. If the prediction is failure, then the go back to second / third step to modified the design / punch path. This process can be iterated several times till the prediction is success. The fixture and the support are made according to the prediction results. Finally, the part is manufactured successfully.

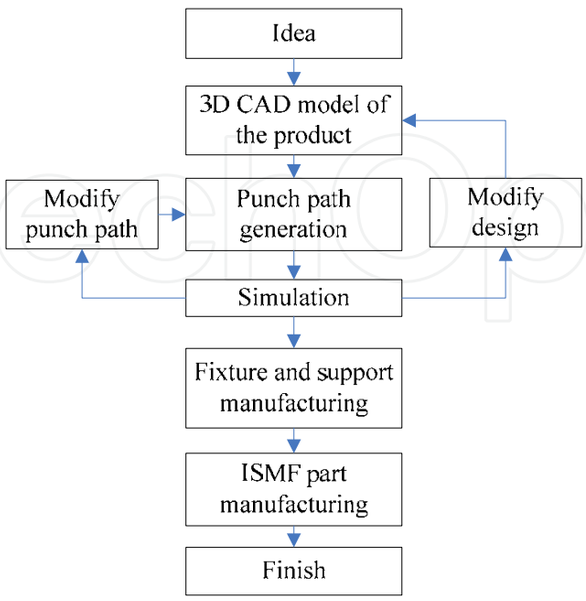


Fig. 11. The proposed ISMF process (Tuomi & Lamminen, 2004)

As we can see that the key to success application of this process to incremental punching process is to be able to predict the deformation and the strain / stress of the part incurred during the forming process. Because of the complexity of the problem, analytical models and solutions may not possible to compute the some processes. It is possible to use commercial FEM packages for establishing quantitative relations between the forming parameters and local deformation of the formed part. But incremental punching is a very complex process in which a huge numbers of contacts between the tool and workpiece (more than say 5000 punches) are involved in forming a typical part. According to our experience, it takes more than 5 days for computing a case with 100 punches. Hence, a fast computing model is required to fulfill the above mentioned process.

4.1 Finding the final shape based on minimum energy principle

As above mentioned, the new incremental punching process can be described as follows: A sheet metal blank is secularly clamped by a blank holder and is incrementally stretched by the punch to reach the final shape punch by punch. In each punch, the punch force is sufficient for the sheet metal to deform. Punches on different locations will result in different amount of deformation. Also, in each punch, the contact region and the blank holder region is constrained. The rest of sheet metal beyond the vicinity of the contact area of the sheet metal are free; however, it may have plastic deformation when its effective stress is large than the yield stress. As a result, for a single punch, its effect region is not only to the contact area, but also the region nearby. As the process goes, the sheet metal attempts to reach a minimum energy state forming the shape. Figure 12 shows a simple case of two punches. The thick line is the geometric profile, while the dash line is the predicted profile. Note that the geometric profile follows the punch positions while the predicted profile is resulted from the minimum energy state of the sheet metal. This method has been used by a number of researchers, such as Tang et al. (2007).

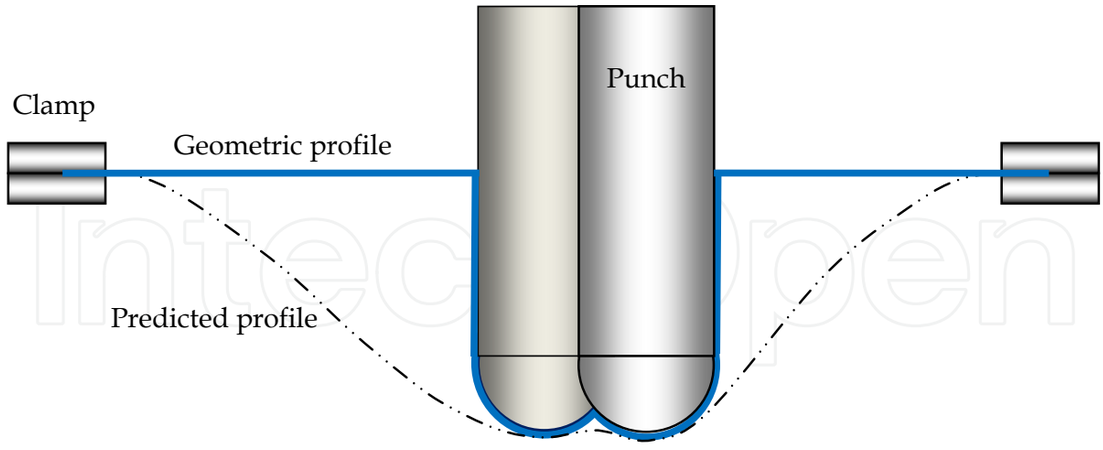


Fig. 12. Illustration of a deformed sheet metal

To model our ISMF process, following assumptions are made:

1. In the entire process, the sheet metal is secularly clamped by the blank holder;
2. Because the punching takes place in a very short period of time, the effect of friction due to the contact between the punch hammer and the sheet metal is negligible (this assumption is the same as the conventional one punch stamping);

3. The initial energy of the sheet metal is zero;
4. The sheet metal blank can be described by its middle surface;
5. The dynamic effect of each punching is negligible (i.e., the vibration of the sheet metal is negligible);
6. The volume of the sheet metal is conserved throughout the process; and
7. The material will not fracture during the process.

As stated in the previous section, during the ISMF process, the sheet metal will deform to its lowest energy state. At the mean time, it must satisfy the boundary conditions, including the geometric surfaces of punches, as well as the clamping condition. Accordingly, the final shape of the surface can be found. To model the mechanics of the process, we firstly define the energy function of the deformed sheet metal. Hu et al. (2001) defined the energy function for NURBS surfaces. It is utilized to model deformed sheet metal here. Denote the middle surface of the sheet metal as $S(x, y)$, the energy function of the deformed sheet metal can be represented as follows:

$$E\left(S(x,y)\right)=\iint\left(\alpha_{11}\frac{\partial S^T}{\partial x}\frac{\partial S}{\partial x}+\alpha_{22}\frac{\partial S^T}{\partial y}\frac{\partial S}{\partial y}+\beta_{11}\frac{\partial^2 S^T}{\partial x^2}\frac{\partial^2 S}{\partial x^2}+\beta_{12}\frac{\partial^2 S^T}{\partial x\partial y}\frac{\partial^2 S}{\partial x\partial y}+\beta_{22}\frac{\partial^2 S^T}{\partial y^2}\frac{\partial^2 S}{\partial y^2}\right)dxdy \quad (6)$$

where, a_{11} is the stretching stiffness in x direction, a_{22} the stretching stiffness in y direction, β_{11} the bending stiffness in x direction, β_{12} the bending stiffness in x and y direction, and β_{22} the bending stiffness in y direction. These parameters can be calculated based on the material properties of the sheet metal.

Although Equation (6) has no analytical solution, it can be solved numerically. Express the surface in discrete grids, the energy function can then be written in discrete form:

$$\begin{aligned}E(S)=&\alpha_{11}\left(\sum_{i,j}^{n,m}\left(\frac{S_{i+1,j}-S_{i,j}}{\Delta x_{i,j}}\right)^2+\sum_{i,j}^{n,m}\left(\frac{S_{i,j}-S_{i-1,j}}{\Delta x_{i,j}}\right)^2\right)\\&+\alpha_{22}\left(\sum_{i,j}^{n,m}\left(\frac{S_{i,j+1}-S_{i,j}}{\Delta y_{i,j}}\right)^2+\sum_{i,j}^{n,m}\left(\frac{S_{i,j}-S_{i,j-1}}{\Delta y_{i,j}}\right)^2\right)\\&+\beta_{11}\cdot\sum_{i,j}^{n,m}\left(\frac{(2\cdot S_{i,j}-S_{i-1,j}-S_{i+1,j}}{\Delta x_{i,j}^2}\right)^2+\beta_{22}\cdot\sum_{i,j}^{n,m}\left(\frac{(2\cdot S_{i,j}-S_{i,j-1}-S_{i,j+1}}{\Delta y_{i,j}^2}\right)^2\\&+\beta_{12}\sum_{i,j}^{n,m}\left(\frac{S_{i+1,j+1}-S_{i-1,j+1}-S_{i+1,j-1}+S_{i-1,j-1}}{4\Delta x_{i,j}\cdot\Delta y_{i,j}}\right)^2\end{aligned} \quad (7)$$

where, n and m are the number of nodes in x and y directions. $\Delta x_{i,j}=\frac{\left|x_{i+1,j}-x_{i-1,j}\right|}{2}$ and $\Delta y_{i,j}=\frac{\left|y_{i,j+1}-y_{i,j-1}\right|}{2}$ are the distances between the nodes in x and y directions respectively (by central difference).

Based on the minimum energy principle, for a point, S_{ij}, not in its lowest energy state, it will be driven to its lowest energy state. From the Equation (7), the energy of S_{ij} is:

$$
\begin{aligned}
E\left(S_{ij}\right) = \alpha_{11}&\left(\left(\frac{S_{i+1,j}-S_{i,j}}{\Delta x_{i,j}}\right)^2+\left(\frac{S_{i,j}-S_{i-1,j}}{\Delta x_{i,j}}\right)^2\right)\\
+\alpha_{22}&\left(\left(\frac{S_{i,j+1}-S_{i,j}}{\Delta y_{i,j}}\right)^2+\left(\frac{S_{i,j}-S_{i,j-1}}{\Delta y_{i,j}}\right)^2\right)\\
+\beta_{11}&\cdot\left(\frac{(2\cdot S_{i,j}-S_{i-1,j}-S_{i+1,j}}{\Delta x_{i,j}^2}\right)^2+\beta_{22}\cdot\left(\frac{(2\cdot S_{i,j}-S_{i,j-1}-S_{i,j+1}}{\Delta y_{i,j}^2}\right)^2\\
+\beta_{12}&\left(\frac{S_{i+1,j+1}-S_{i-1,j+1}-S_{i+1,j-1}+S_{i-1,j-1}}{4\Delta x_{i,j}\cdot\Delta y_{i,j}}\right)^2
\end{aligned}
\tag{8}
$$

The resulting force on the node is:

$$
\begin{aligned}
F_{ij} = \frac{\partial E\left(S_{ij}\right)}{\partial S_{ij}} &= 2\alpha_{11}\frac{2S_{i,j}-S_{i+1,j}-S_{i-1,j}}{\Delta x_{i,j}^2}+2\alpha_{22}\frac{2S_{i,j}-S_{i+1,j}-S_{i-1,j}}{\Delta y_{i,j}^2}\\
&+2\beta_{11}\cdot\frac{2\cdot S_{i,j}-S_{i-1,j}-S_{i+1,j}}{\Delta x_{i,j}^4}+2\beta_{22}\cdot\frac{2\cdot S_{i,j}-S_{i,j-1}-S_{i,j+1}}{\Delta y_{i,j}^2}
\end{aligned}
\tag{9}
$$

Using Equation (9), the minimum energy state of S_{ij}, can be found through iterative searching:

$$
S_{ij}(t) = S_{ij}(t-1) + c\cdot F_{ij}(t-1) \tag{10}
$$

where, t is the times of iterations, c is a positive constant, the driven force, F_{ij} is positive in the positive direction of z.

Note that some points are constrained by the boundary conditions, including the contacting points of the punch, and the contacting points to the blank holder. These points will be invariant in the process. In addition, Equation (10) assumes the minimum energy state, S'_{ij}, has the same position as S_{ij} in x and y directions. This may cause some error. However, the error shall be small when the forming angle in z direction is less than 70^o.

4.2 Finding the strain / stress distribution using inverse FEM

The other major concern is the strain and stress incurred in the forming process. Overstress may cause the sheet metal fracture and hence, shall be avoided. We use the inverse FEM, also called the one-step FEM, to compute the strains and the stresses. Different from the conventional FEM, it simulates the entire sheet metal forming process in one-step and hence, is very fast; though its accuracy is not as good. According to literatures, Batoz et al. (1998) first developed an inverse FEM approach with simple triangular shell elements. Lee and Huh (1998) introduced a new inverse FEM approach to predict blank shape and strain distribution. More recently, Du et al. (2006) discussed several important issues in inverse FEM. Lan et al. (2005) derived a new model to predict the thickness strain distribution. These research results lay the foundation for our research.

In our ISMF process, the part is formed punch by punch. In each punch, there is deformation (both plastic and elastic), stress build-up and strain-hardening. In addition, the

result of each punch is dependent on the previous punches. However, the final shape of the part shall follow the minimum energy state. Based on the final shape of the part, the inverse FEM can predict the thickness strain distribution with reasonable accuracy.

4.2.1 The kinematics of the inverse FEM

In order to simplify the problem, it is assumed that the strain is membrane strain and the thickness is perpendicular to the sheet metal surface. In addition, the effect of elastic deformation is negligible. Following the discussion above, the minimum energy state is used as the final shape. To find the strain and the stress, the inverse FEM starts from the final shape and projects the final shape back to the sheet metal blank. The difference between the projection and the original shape is caused by the deformation and hence, can be used to compute the strain and stress.

Figure 13 shows the geometric relation of a typical element on the final shape and its project (the guess solution) on the blank. It should be noted that the guess solution is an approximation of the actually 'initial states'. The two states is essentially a transformation between the part coordinate system *(x, y, z)* (the local coordinate system) and the original blank coordinate system *(X, Y, Z)* (the global coordinate system). Assume the element is a three-node triangle with straight sides (the so-called Constant Strain Triangle or CST), then, the elongation strain distribution of the element can be computed as shown below (Reddy & Reddy, 2007).

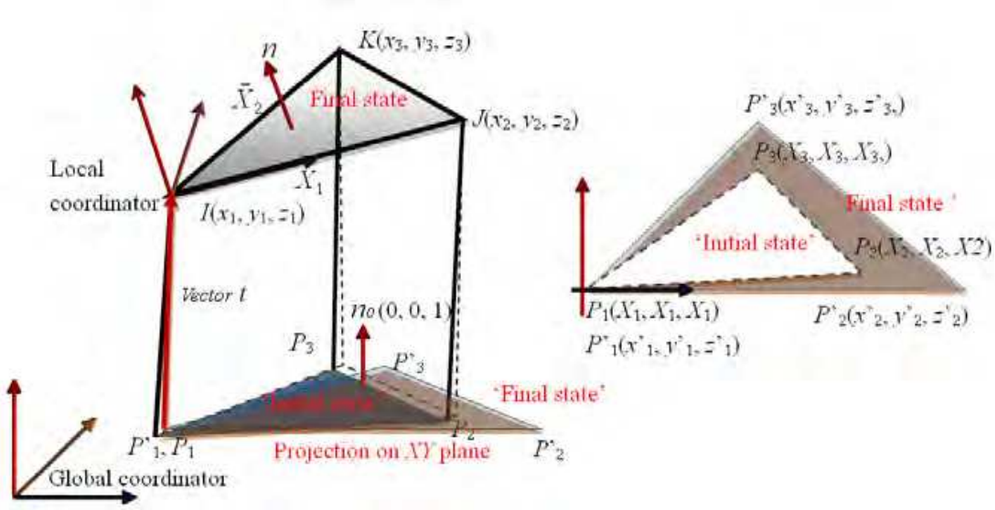


Fig. 13. Illustration of the mapping in the inverse FEM

First, as shown in the figure, the upper element is the 'final state' and the lower element is taken as the 'initial state'. The initial state is in the XY plane, and its normal vector is n0 = (0, 0, 1). On the other hand, the normal vector of the final state element in the global coordinator is:

$$n = \bar{X}_1 \times \bar{X}_2 = K_x i + K_y j + K_z k \tag{11}$$

where, $\bar{X}_1$ and $\bar{X}_2$ are the vectors of the two edges of the final state element. They can be expressed as follows:

$$\vec{X}_1 = J - I = \langle (x_2 - x_1), (y_2 - y_1), (z_2 - z_1) \rangle$$

$$\vec{X}_2 = K - I = \langle (x_3 - x_1), (y_3 - y_1), (z_3 - z_1) \rangle \tag{12}$$

Moreover, the angels between the two elements in the YZ plane, a, and the XZ plane, β, can be described by using the two normal vectors:

$$\alpha = \arccos \frac{\langle K_y, K_z \rangle \cdot \langle 0,1 \rangle}{|\langle K_y, K_z \rangle| \cdot |\langle 0,1 \rangle|} \tag{13}$$

$$\beta = \arccos \frac{< K_x, K_z > \cdot < 0,1 >}{|< K_x, K_z >| \cdot |< 0,1 >|} \tag{14}$$

Though, since n_0 is perpendicular to the XY plane, it cannot be used to compute the angel in the XY plane. Fortunately, the angle can be found by using the two vectors $\vec{x}_1$ and $\vec{X}_1$, which are the first edges of elements in the initial and the final states.

$$\theta = \arccos \frac{< (x_2 - x_1), (y_2 - y_1) > \cdot < (X_2 - X_1), (Y_2 - Y_1) >}{|< (x_2 - x_1), (y_2 - y_1) >| \cdot |< (X_2 - X_1), (Y_2 - Y_1) >|} \tag{15}$$

With the three angles, the rotation matrix can then be found:

$$[R] = \begin{bmatrix} r_{xx} & r_{xy} & r_{xz} \\ r_{yx} & r_{yy} & r_{yz} \\ r_{zx} & r_{zy} & r_{zz} \end{bmatrix} \tag{16}$$

where,

$r_{xx} = \cos\beta\cos\theta$

$r_{xy} = \sin\alpha\sin\beta\cos\theta - \cos\alpha\sin\theta$

$r_{xz} = \cos\alpha\sin\beta\cos\theta + \cos\alpha\sin\theta$

$r_{yx} = \sin\alpha\sin\beta\cos\theta - \cos\alpha\sin\theta$

$r_{yy} = \cos\theta\sin\theta$

$r_{yz} = \cos\alpha\sin\beta\sin\theta - \cos\alpha\sin\theta$

$r_{zx} = -\sin\beta$

$r_{zy} = \sin\alpha\cos\beta$

$r_{zz} = \cos\alpha\cos\theta$

To compute the strain, the coordinate system of the final state needs to align to the coordinate system of the initial state. This requires the movement X_i' expressed below:

$$X_i' = [R] X_i + \vec{t} \tag{17}$$

where, X_i, $i = 1, 2, 3$, are position of the node in final state; $\vec{t}$ is the vector of the translation of the fist node between final state and the initial state.
Having aligned the finial state element in the XY plane, the element can be then considered as a 2D element (since z_i' are 0). In this case, the displacement $[u]$, the true strains $[\lambda]$, and the stresses $[\sigma]$ are defined as [26]:

$$[u]=\begin{bmatrix} u_x \\ u_y \end{bmatrix}; \quad [\lambda]=\begin{bmatrix} \lambda_{xx} \\ \lambda_{yy} \\ \lambda_{zz} \end{bmatrix}; \quad [\sigma]=\begin{bmatrix} \sigma_{xx} \\ \sigma_{yy} \\ \sigma_{zz} \end{bmatrix} \tag{18}$$

Since the element is CST, the displacement will be linear over the element. The displacements in terms of x and y can be written as:

$$\begin{aligned} u_x(x,y) &= W_1 + W_2 x + W_3 y \\ u_y(x,y) &= W_4 + W_5 x + W_6 y \end{aligned} \tag{19}$$

where, W_i are the constants.
The displacement of the element can be expressed as:

$$[u]=\begin{bmatrix} u_{x1} \\ u_{y1} \\ u_{x2} \\ u_{y2} \\ u_{x3} \\ u_{y3} \end{bmatrix}=\begin{bmatrix} x_1'-x_1 \\ y_1'-y_1 \\ x_2'-x_2 \\ y_2'-y_2 \\ x_3'-x_3 \\ y_3'-y_3 \end{bmatrix} \tag{20}$$

Or:

$$\begin{bmatrix} u_{x1} \\ u_{y1} \\ u_{x2} \\ u_{y2} \\ u_{x3} \\ u_{y3} \end{bmatrix}=\begin{bmatrix} 1 & x_1 & y_1 & 0 & 0 & 0 \\ 0 & 0 & 0 & 1 & x_1 & y_1 \\ 1 & x_2 & y_2 & 0 & 0 & 0 \\ 0 & 0 & 0 & 1 & x_2 & y_2 \\ 1 & x_3 & y_3 & 0 & 0 & 0 \\ 0 & 0 & 0 & 1 & x_3 & y_3 \end{bmatrix}\begin{bmatrix} W_1 \\ W_2 \\ W_3 \\ W_4 \\ W_5 \\ W_6 \end{bmatrix} \tag{21}$$

Furthermore, Equation (21) can be abbreviated to:

$$[u]=[A][W] \tag{22}$$

where, $[A]$ is the shape matrix of the initial element, and $[W]$ is the constants matrix. The constants matrix can be solved using the following equation:

$$[W]=\left[A^{-1}\right][u] \tag{23}$$

Based on the definition of strains and displacement, the element strains can be determined as follows:

$$\begin{bmatrix} \lambda_{xx} \\ \lambda_{yy} \\ \lambda_{xy} \end{bmatrix} = \begin{bmatrix} \dfrac{\partial u_x}{\partial x} \\ \dfrac{\partial u_y}{\partial y} \\ \dfrac{\partial u_y}{\partial x} + \dfrac{\partial u_x}{\partial y} \end{bmatrix} = \begin{bmatrix} W_2 \\ W_6 \\ W_3 + W_5 \end{bmatrix} \tag{24}$$

The direction of the principle strains is given by:

$$\varphi = \frac{1}{2}\arctan\frac{2\lambda_{xy}}{\lambda_{xx} - \lambda_{yy}} \tag{25}$$

so that,

$$[m] = \begin{bmatrix} \cos\varphi & \sin\varphi & 0 \\ -\sin\varphi & \cos\varphi & 0 \\ 0 & 0 & 1 \end{bmatrix} \tag{26}$$

Hence, the principle strain is:

$$\begin{bmatrix} \lambda_1 \\ \lambda_2 \\ \lambda_3 \end{bmatrix} = \left[m^{-1}\right][\lambda]\left[m^{-1}\right]^T \tag{27}$$

To expressed large deformation in sheet metal forming, the logarithmic strain is usually used. It can be expressed as:

$$[\varepsilon] = \begin{bmatrix} \varepsilon_1 \\ \varepsilon_2 \\ \varepsilon_3 \end{bmatrix} = \begin{bmatrix} \ln\lambda_1 \\ \ln\lambda_2 \\ \ln\lambda_3 \end{bmatrix} \tag{28}$$

The logarithmic strain in the local coordinator is:

$$\begin{bmatrix} \varepsilon_{xx} & \varepsilon_{xy} & 0 \\ \varepsilon_{xy} & \varepsilon_{yy} & 0 \\ 0 & 0 & \varepsilon_{zz} \end{bmatrix} = [m][\varepsilon][m]^T \tag{29}$$

4.2.2 Material continuation descriptions and stress

As the inverse FEM only considers the 'initial state' and the 'final state' of the sheet metal, the resultant strain is independent from the loading history. Thus, the assumption of

proportional loading is applied. According to Hency-Ilyushin's law, the Hill's anisotropic yield criterion can be written as:

$$f(\sigma)=[\sigma][P][\sigma]^T-\bar{\sigma}^2=0 \tag{30}$$

where $[\sigma]=\begin{bmatrix}\sigma_{xx} & \sigma_{yy} & \sigma_{xy}\end{bmatrix}$ is the Cauchy plane stress, and $\bar{\sigma}$ is the equivalent stress. With the Lankford value r , the anisotropic matrix can be written as:

$$[P]=\begin{bmatrix}1 & -\frac{r}{1+r} & 0\\ -\frac{r}{1+r} & 1 & 0\\ 0 & 0 & \frac{2(1+2r)}{1+r}\end{bmatrix} \tag{31}$$

By using the Hencky proportional deformation theory, the plastic strain can be gotten as:

$$\bar{\varepsilon}=\left\{[\varepsilon][P][\varepsilon]^T\right\}^{\frac{1}{2}} \tag{32}$$

where, $[\varepsilon]=\begin{bmatrix}\varepsilon_{xx} & \varepsilon_{yy} & \varepsilon_{xy}\end{bmatrix}$. Suppose the material is subject to the pre-strain constant law as follow:

$$\bar{\sigma}=K\left(\varepsilon_0+\bar{\varepsilon}\right)^n$$

In the presented study only normal anisotropy is taken into account, and thus the constitutive relation is as follows:

$$[\sigma]^T=\frac{\bar{\sigma}}{\bar{\varepsilon}+\varepsilon_0}[P]^{-1}[\varepsilon]^T \tag{34}$$

This gives the stress distribution of the part.

5. Experiment results

Using the new machine, a large number of experiments were carried out. In this section, two experiments are presented in details. In both experiments, the workpiece material is SPCC steel. The size of the punch we applied here is 10*mm*. The material properties are summarized as follows:

Workpiece size	300.0 × 300.0 *mm*;
Workpiece thickness	h_0 =1 *mm*;
Yang's module	E = 206.0*GPa* ;
Poisson ratio	v = 0.3;
Stress-strain hardening curve	$\sigma=576\cdot(1.0\times10^{-4}+\bar{\varepsilon}_p)^{0.23}$MPa ($\bar{\varepsilon}_p$ is the effective strain);
Lankford value	r =1.87;

5.1 Example 1

In this example, two parts were made with the Setup A and Setup B. The design of the part is same, as shown in Figure 14; however, different control parameters are used. In Case A, the layer thickness is 1 mm and the feed step varies from 1mm to 4mm. In Case B, The layer thickness is 3 mm and the feed step is uniform (3mm). Figure 14 shows the simulation and experiment results, in which (a) is the punch path, (b) is the geometric surface based on the punch path, (c) is the predicted part surface using the minimum energy method, (d) is the predicted thickness strain distribution using the inverse FEA method, and (e) is the experiment results. It is interesting to note that the center of the part is not being punched. Though, it deforms to its lowest energy position as predicted. Moreover, both cases result in similar thickness strain distribution. However, the part in Case B has large punch marks, as predicted. From the figure, it is seen that the computer simulations and the experiment results are well matched.

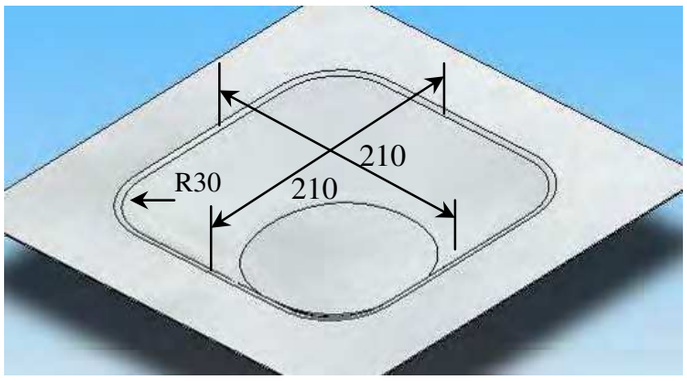
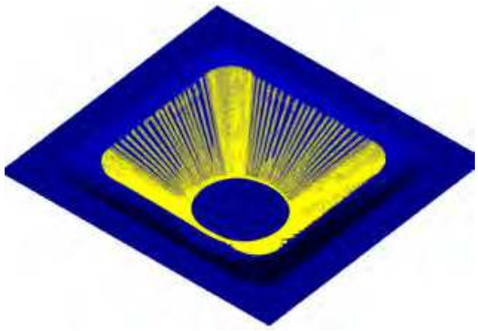


Fig. 14. CAD model of the tank (unit: mm)

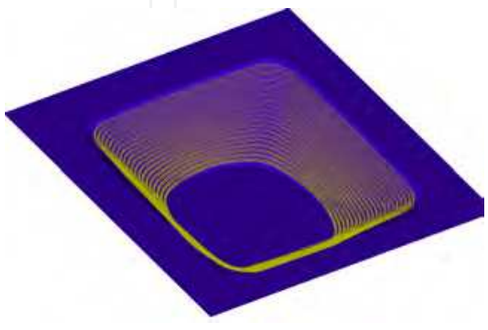
Figures 16 and 17 show more detailed studies. We first select a cross section as shown in Figure 15, and then measure the geometry using a CMM machine. From Figure 16, it is seen that the part quality in Case A is better. This is because the uniform step size is not as effective as the variable step size, which can better accommodate the curvatures. In both cases, the experiment results match the simulation results very well, though in comparing to the design, they both have significant errors around the edges. It is noted that the error in Case B is large because of the offset in holding the sheet metal blank. Also, it is seen that at

Case A

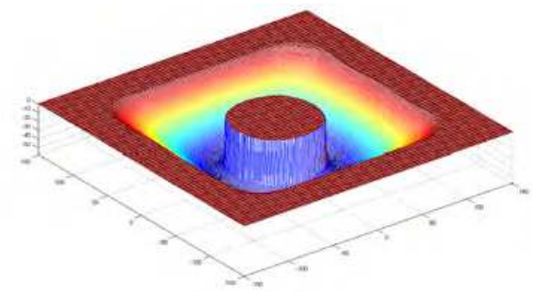


(a1) Punch path in Case A

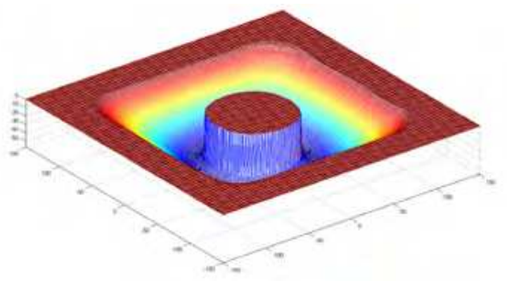
Case B



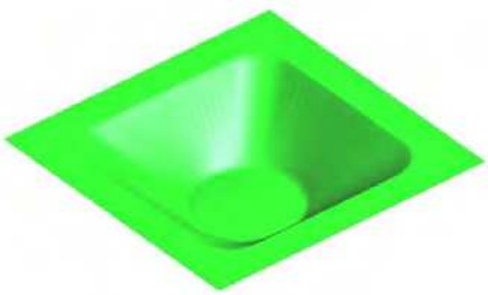
(b1) Punch path in Case B



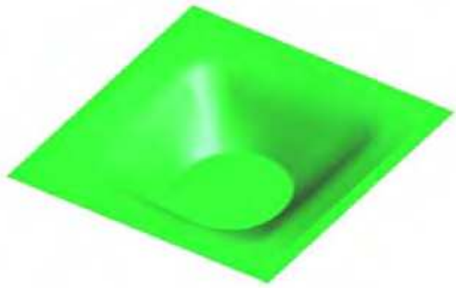
(a2) Geometric surface based on the punch path in Case A



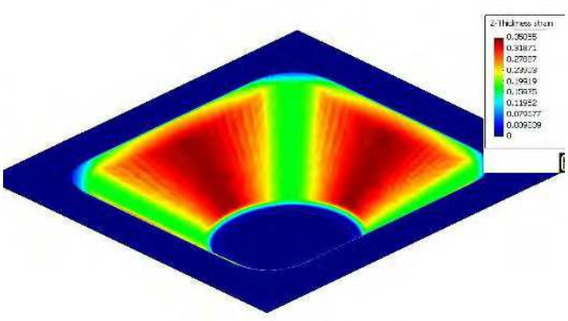
(b2) Geometric surface based on the punch path in Case B



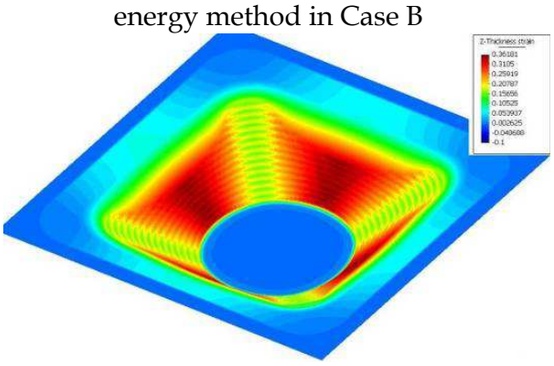
(a3) Predicted surface based on minimum energy method in Case A



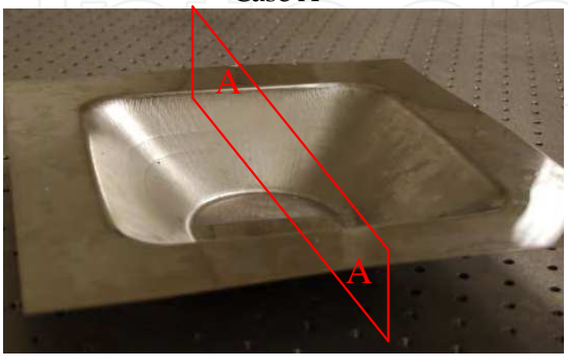
(b3) Predicted surface based on minimum energy method in Case B



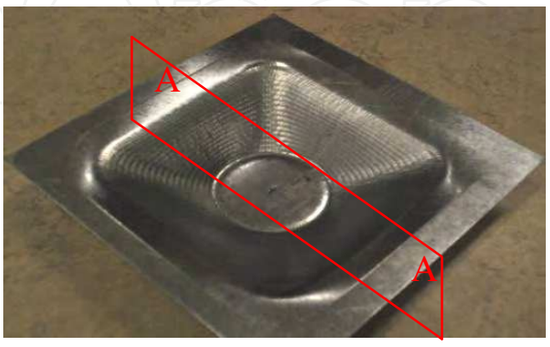
(a4) The thickness strain distribution in Case A



(b4) The thickness strain distribution in Case B



(a5) The experimental result in Case A



(b5) The experimental result in Case B

Fig. 15. Experiment results in Example 1

the bottom of the part, there is a blending. Causing by the stress of the metal, the blending is unfortunately unavoidable. Figure 17 shows the errors along the cross section. From the figure, it is seen that the maximum error occurs where the curvatures is the largest. In the other regions, the error is less than 2 mm.

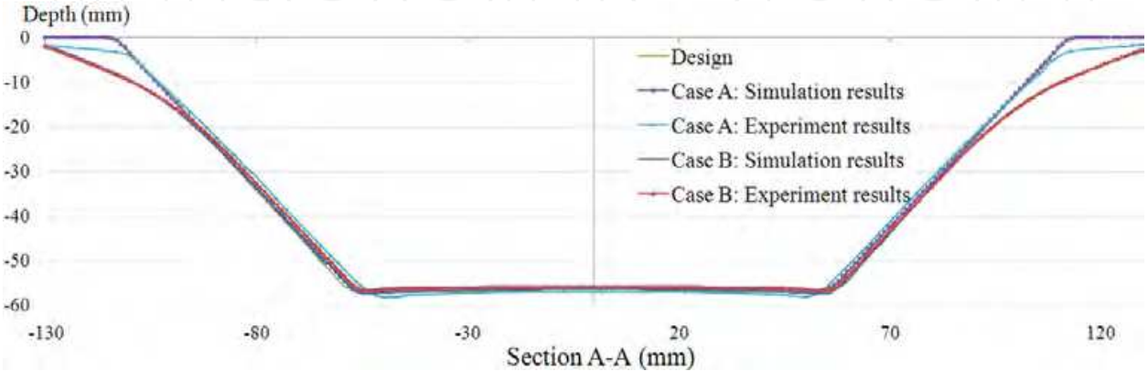


Fig. 16. The cross section geometric profile of the parts

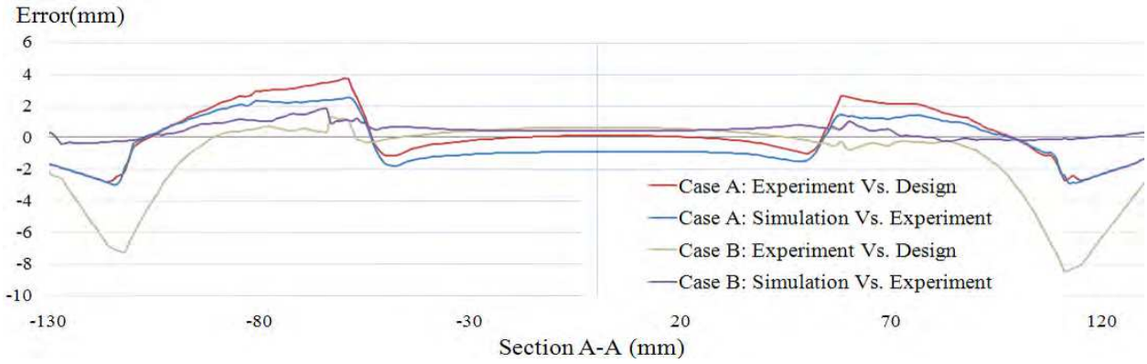
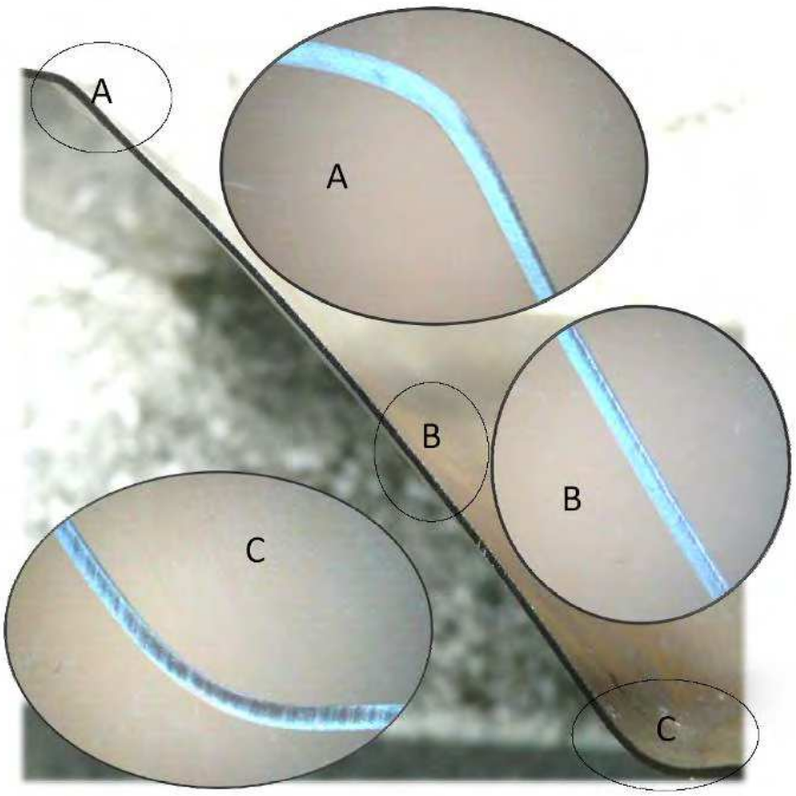
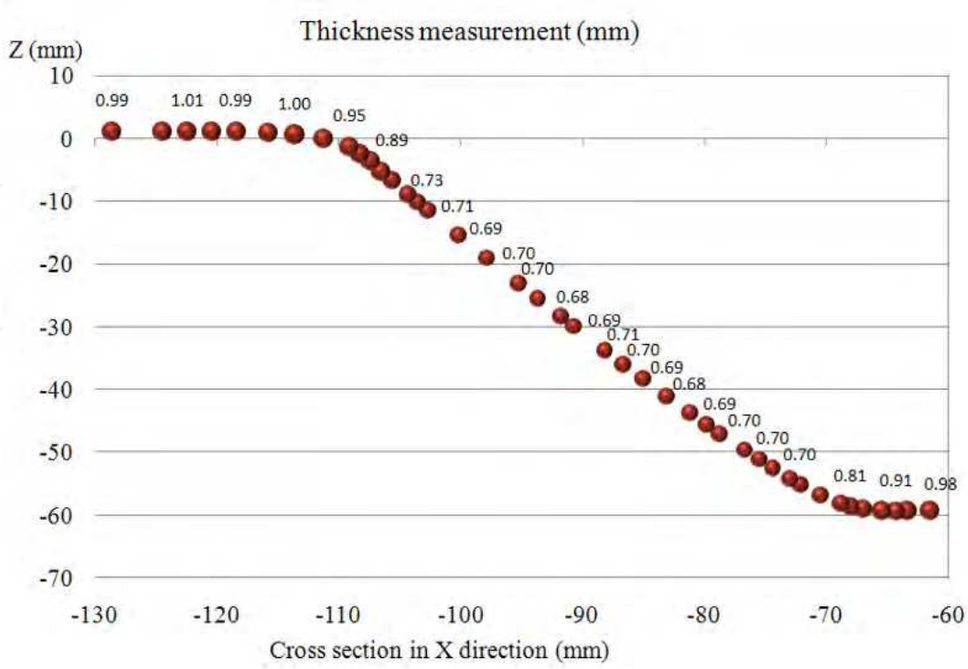


Fig. 17. The cross section error distributions of the parts

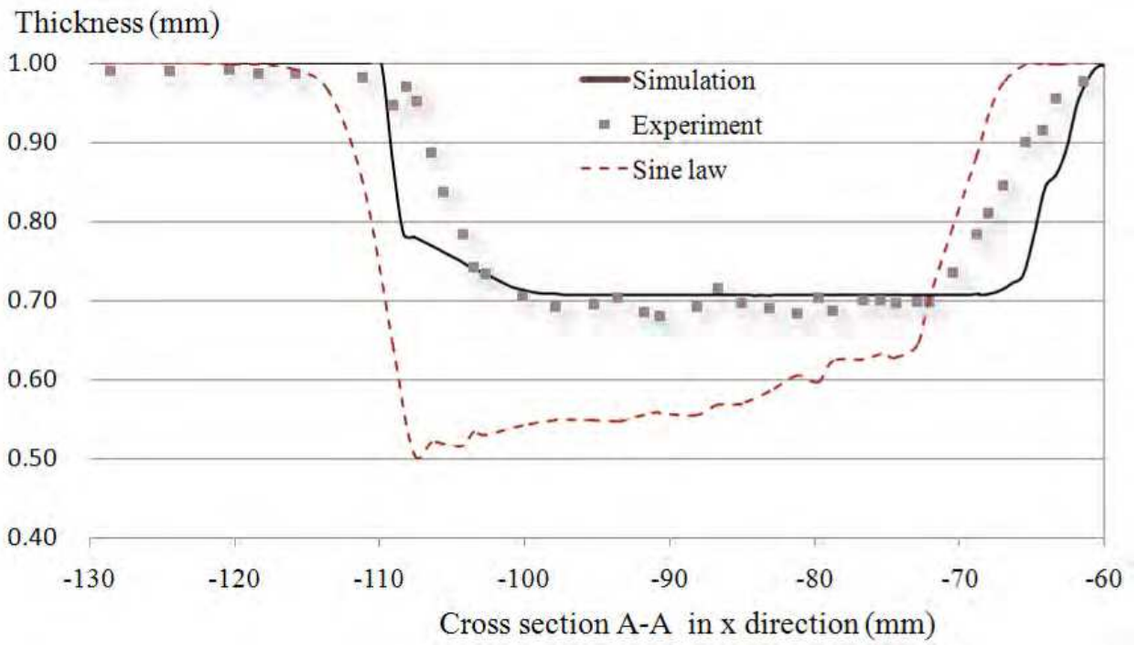
Figure 18 shows the cross section and the thickness measurements.



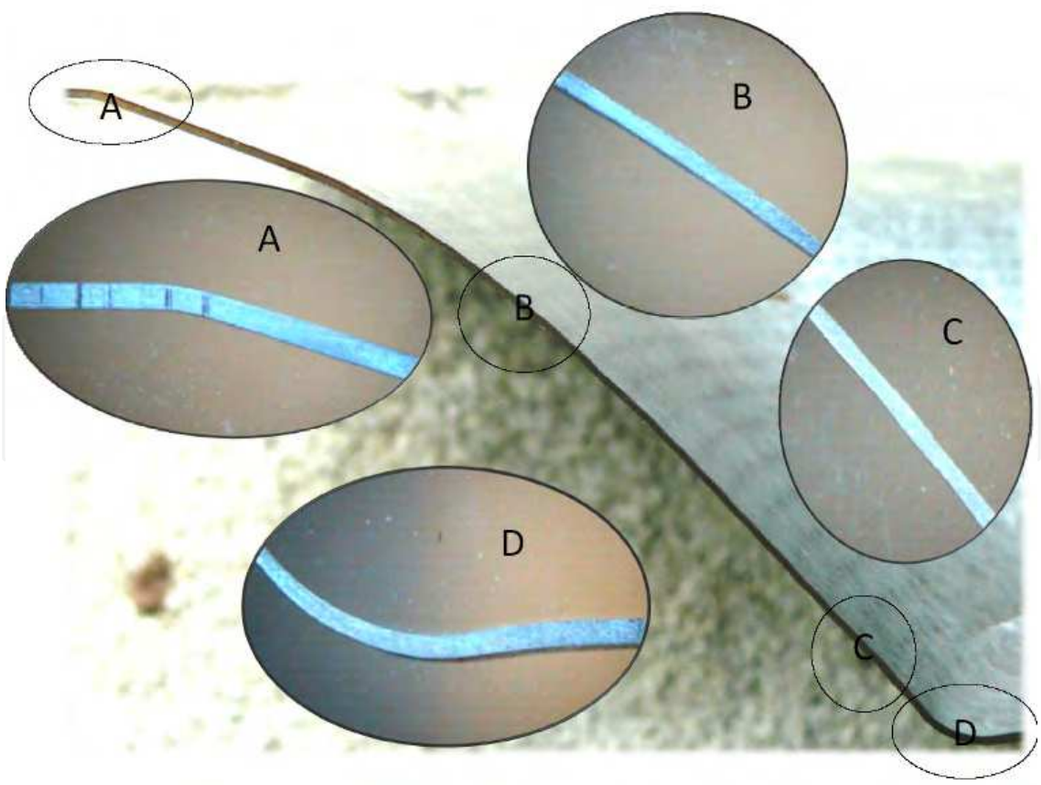
a) Section views in Case A



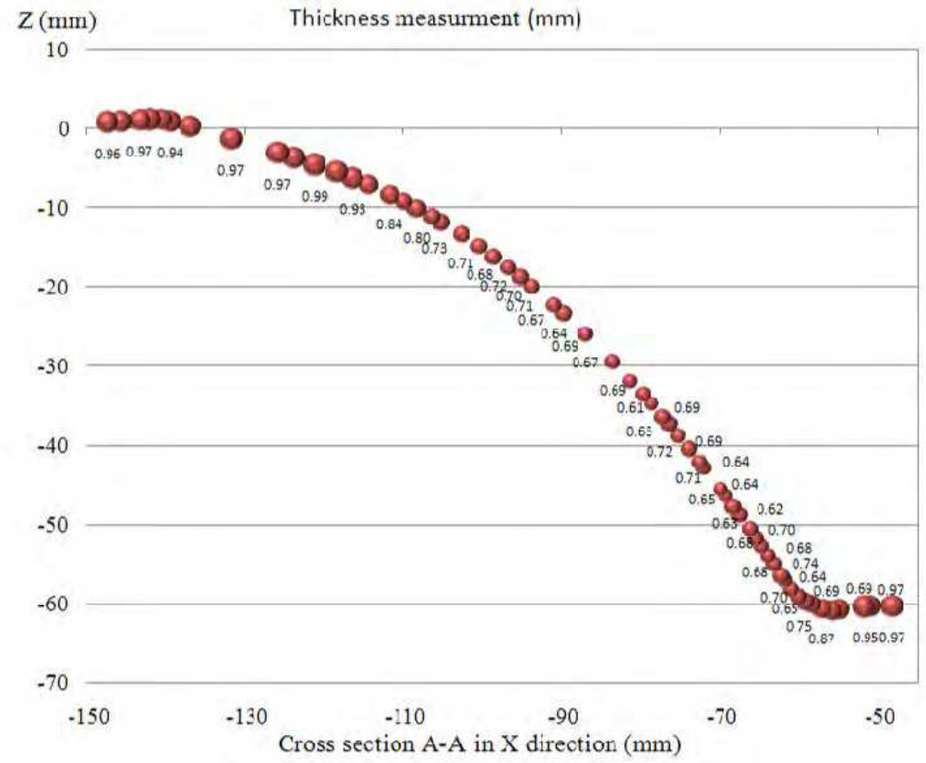
b) Thickness measurement in Case A



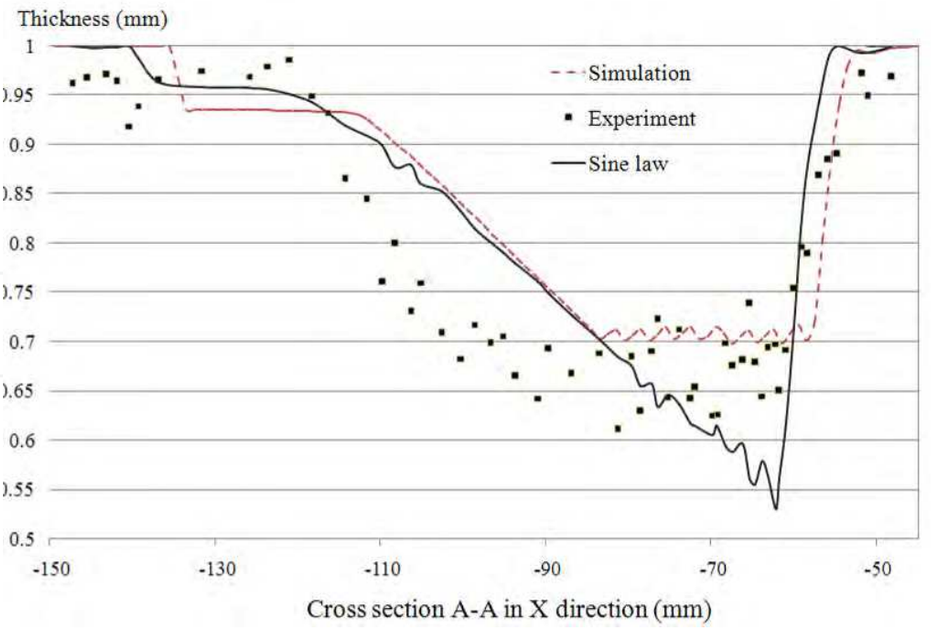
c) Comparison of the thickness distribution in cross section A-A: Simulation, sine law and experiment



d) Cross section views in Case B



e) Thickness measurement in Case B



f) Comparison of the thickness distribution in cross section A-A: Simulation, sine law and experiment

Fig. 18. The cross section thickness measurements

5.2 Example 2

The second example is a face mask as shown in Figure 19. Its shape is much more complex containing multiple peaks and valleys. Two experiments are conducted using different blank holders: Case A uses a small blank holder while Case B uses a large blank holder. Though, the punch path is the same as shown in Figure 20 and hence, the geometric surface is the same as shown in Figure 21. The use of different blank holders results in different boundary conditions, and hence, different results. Figure 22 shows the experiment results of the two cases. From the figure, it is seen that the computer simulation matches the experiment result well. In addition, it is seen that Case A will result in a fracture, which is proved experimentally. This is because the deformation of the sheet metal exceeds its forming limit in this region.



Fig. 19. The design of Example 2

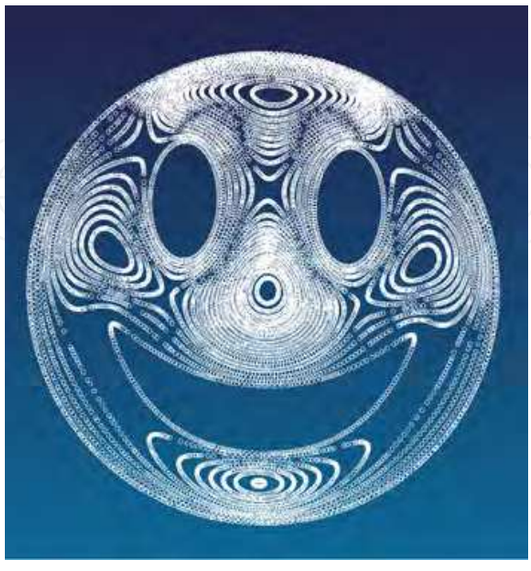


Fig. 20. The punch path of Example 2

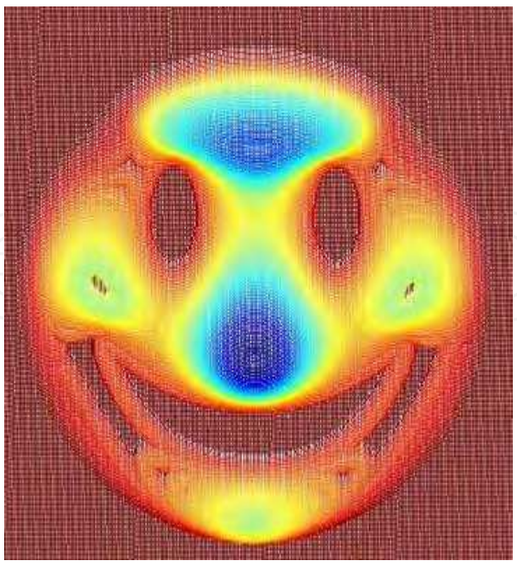


Fig. 21. The geometric surface of Example 2

Figure 23 shows a more detailed study on the cross section along the center line of the mask in Case B. From the figure, it is seen that the computer simulation matches the experiment results well. Though, in comparing to the design, they both have a significant error (about 15 mm) around the edges. Figure 24 shows the error between experiment and simulation of the cross section. To reduce the error, additional research is needed.

6. Maximum forming angle

In sheet metal forming, the formability is an important concern. The formability is expressed as the maximum forming angle, θmax, that a sheet would endure without fracturing. Gao et al. designed a new method to evaluate the forming angle (Cui & Gao, 2009). Jeswiet et al. (2007) summarized the maximum forming angle in CNC ISMF and Robot ISMF. According to literatures, the maximum forming angle of an 1mm mild steel sheet of DC04 is about 65o. In this study, we used SPCC which has similar mechanical properties as that of DC04.
In this test, the vertical feed rate (the layer thickness) is set at 1 mm, the horizontal feed rate is set 1 mm and the punch diameter is 10 mm. The blank thickness is 1 mm and the size is 150.0 × 150.0 mm. The size of the fixture is 80.0 × 80.0 mm. The experiment setup is shown in Figure 25. The experiment results are summarized in Figure 26. The testing result is rather similar to that of in the reference done by Jeswiet et al. (2007).
The final thickness of the sheet metal can be computed by the forming angle using the Sine law:

$$t = t_0 \sin(\frac{\pi}{2} - \theta) \tag{34}$$

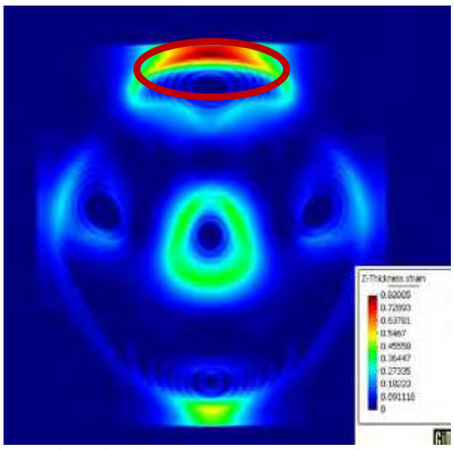
where, t0 is the initial thickness of the blank, θ is the forming angle.



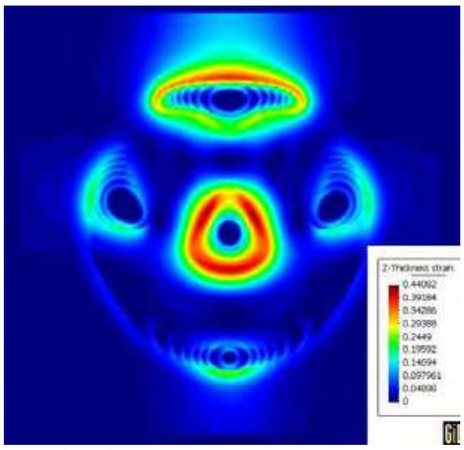
(a1) Predicted surface in Case A



(b1) Predicted surface in Case B



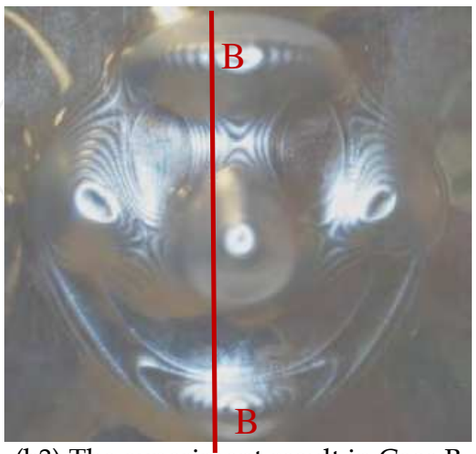
(a2) The thickness strain distribution in Case A



(b2) The thickness strain distribution in Case B



(a3) The experiment result in Case A



(b3) The experiment result in Case B

Fig. 22. The experiment results of Example 2

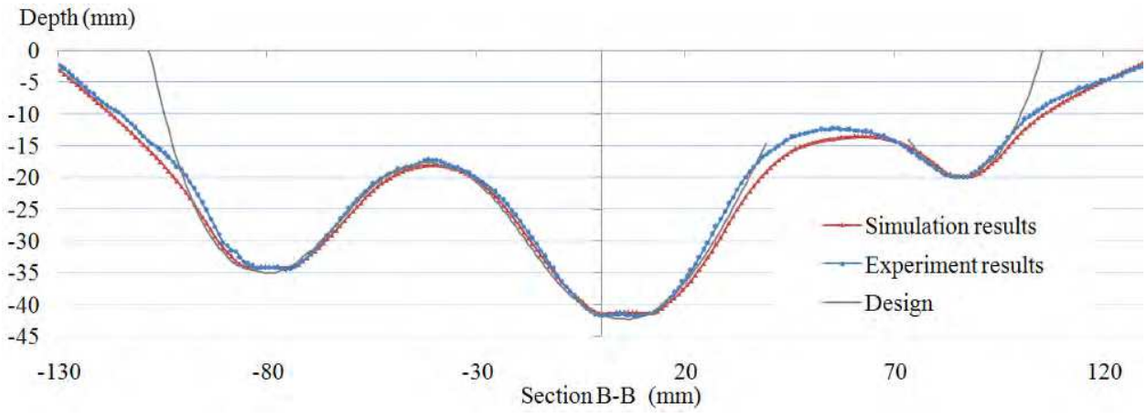


Fig. 23. A comparison of computer simulation and experimental result in Example 2

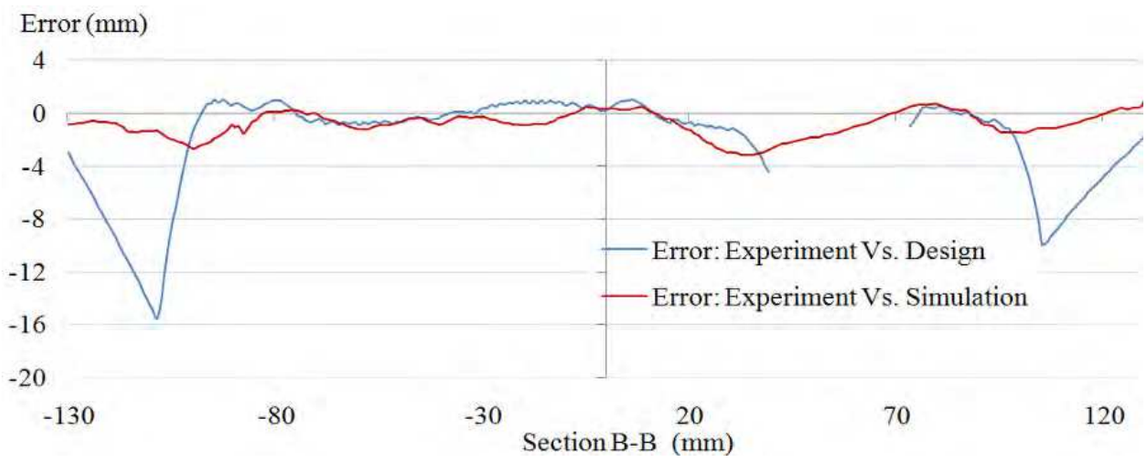
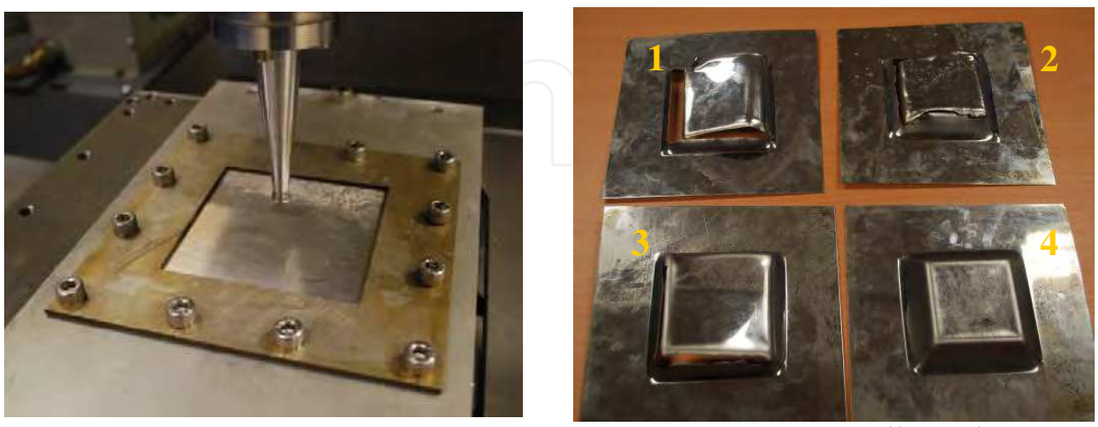


Fig. 24. Error distributions along the cross section in Example 2



(a) Configuration of the test

(b) Testing part with different forming angle: 1 – 80o; 2 – 75o, 3 – 68o, 4 –63o

Fig. 25. The experiments for testing the formability of SPCC

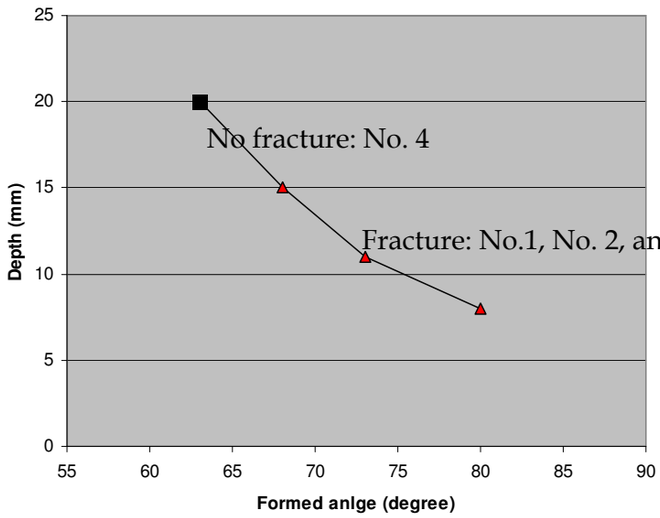


Fig. 26. The maximum forming angle test results

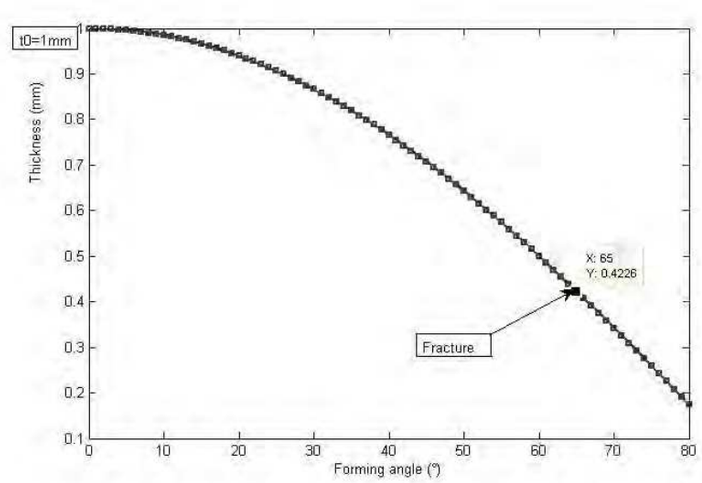


Fig. 27. The predicted thickness using Sine law

7. Conclusions and future work

The Chapter is focused on the design and building of an ISMF machine, theoretical study of the forming process, as well as experiment testing. Based on the results presented above, following conclusions can be drawn:

1. The presented ISMF method is effective in making free form sheet metal parts.
2. The mechanics model can predict the part surface as well as the thickness strain distributions. The prediction error is usually well within 2 to 3 mm. Though, there could be a significant error around the edges depending on the holding of the sheet metal blank. The computation can usually be done in several minutes using a PC computer.
3. The experiment results match the simulation result well.

4. The success of incremental punching may depend on blank holding.
5. The stamping error can be reduced by adopting adaptive feed step sizes.

With its flexibility and easy operation, it is expected that the presented new method will find many applications in the near future.

Also, it should be pointed out that the presented research is a beginning on developing a viable technology for ISMF. The future work includes:

6. Conducting theoretical study on the forming limit;
7. Studying the effects of spring-back; and
8. Designing and building a flexible bottom support to improve the accuracy of the part.

8. Acknowledgement

The presented research is partially supported by a grant from University Grants Council of Hong Kong under the grant No. 44P5014 and China Fundamental Research Funds for Central Universities under the Project No. CDJRC10110009.

9. References

Lima, P.; Bonarini, A. & Mataric, M. (2004). *Application of Machine Learning,* InTech, ISBN 978-953-7619-34-3, Vienna, Austria

Li, B.; Xu, Y. & Choi, J. (1996). Applying Machine Learning Techniques, *Proceedings of ASME 2010 4th International Conference on Energy Sustainability*, pp. 14-17, ISBN 842-6508-23-3, Phoenix, Arizona, USA, May 17-22, 2010

Siegwart, R. (2001). Indirect Manipulation of a Sphere on a Flat Disk Using Force Information. *International Journal of Advanced Robotic Systems,* Vol.6, No.4, (December 2009), pp. 12-16, ISSN 1729-8806

Arai, T. & Kragic, D. (1999). Variability of Wind and Wind Power, In. *Wind Power,* S.M. Muyeen, (Ed.), 289-321, Scyio, ISBN 978-953-7619-81-7, Vukovar, Croatia

Van der Linden, S. (June 2010). Integrating Wind Turbine Generators (WTG's) with Energy Storage, In. *Wind Power,* 17.06.2010, Available from http.//sciyo.com/articles/show/title/wind-power-integrating-wind-turbine-generators-wtg-s-with-energy-storage

Nakajima, N. (1979). Numerical control for traditional manual forming of sheet metal. *Journal of the Japan Society for Technology of Plasticity*, Vol.23, pp. 696–700.

Mori, K.; Yamamoto, M. & Osakada K. (1996). Determination of hammering sequence in incremental sheet metal forming using a genetic algorithm. *Journal of Materials Processing Technology*, Vol. 60, pp.463–468.

Saotome, Y. & Okamoto, T. (2001). In-situ incremental microforming system for three-dimensional shell structures of foil materials. *Journal of Materials Processing Technology*, Vol. 113, pp. 636–640.

Schafer, T. and Schraft, R. D. (2005). Incremental sheet metal forming by industrial robots,. *Rapid Prototyping Journal*, Vol.11, pp. 278-286.

Callegari, M.; Gabrielli, A. & *et al*. (2008). Incremental Forming of Sheet Metal by Means of Parallel Kinematics Machines. *Journal of Manufacturing Science and Engineering*, Vol. 130(5), paper No.054501.

Amino, H. & Ro, G. (2001). Dieless NC forming. *Journal of the Japan Society for Technology of Plasticity*, Vol. 42, pp. 69–73.

Kopac, J. & Campus, Z. (2005). Incremental sheet metal forming on CNC milling machine-tool. *Journal of Materials Processing Technology*, Vol.162–163, pp 622–628.

Park, J. J. & Kim, Y. H. (2003). Fundamental studies on the incremental sheet metal forming technique. *Journal of Materials Processing Technology*, Vol. 140, pp447–453.

Ceretti E.; Giardini C. and Attanasio A. (2004) Experimental and simulative results in sheet incremental forming on CNC machines. *Journal of Materials Processing Technology*, Vol. 152, pp176–184.

Micari, F.; Ambrogio, G. & Filice, L. (2007). Shape and dimensional accuracy in Single Point Incremental Forming: State of the art and future trends. *Journal of Materials Processing Technology*, Vol. 191, pp. 390-395.

Ham M. and Jeswiet J. (2007). Forming Limit Curves in Single Point Incremental Forming. *CIRP Annals - Manufacturing Technology*, Vol. 56, pp277-280.

Silva, M.B.; Skjoedt, M. & et al. (2009). Single point incremental forming of tailored blanks produced by friction stir welding, Journal of Materials Processing Technology, Vol. 209, pp811-820

Hirt, G.; Ames, J. & et al. (2003). Forming Strategies and Process Modelling for CNC Incremental Sheet Forming. *CIRP Annals – Manufacturing Technology*, Vol. 53, pp. 203–206.

Allwood, J. M.; Music O. & et al. (2009). Closed-loop feedback control of product properties in flexible metal forming processes with mobile tools. *CIRP Annals - Manufacturing Technology* , Vol. 58, pp287-290.

Callegari, M.; Amodio, O. & et al. (2007). Sheet Incremental Forming: Advantages of Robotised Cells vs. CNC Machines. *Industrial Robotics: Programming, Simulation and Application*, ARS, Vienna, pp. 493–514.

Amino Co., (2011) Available from http://www.amino.co.jp/en/products/243.html (last acessed on 2011-04-02).

Luo, Y.; He, K. & Du R. (2010). A New Sheet Metal Forming Method Based on the Incremental Punching, Part 1: Mechanics Model and Simulation. *International Journal of Advanced Manufacturing Technology*, Vol. 51, No.5-8, 481-491.

Luo, Y.; He, K. & Du, R. (2010). A New Sheet Metal Forming Method Based on the Incremental Punching, Part 2: Machine Building and Experiment Results. *International Journal of Advanced Manufacturing Technology*, Vol. 51, No.5-8, 493-506.

Tuomi, J. & Lamminen, L. (2004). Incremental sheet forming as a method for sheet metal component prototyping and manufacturing, *Proceeding of 10th European Forum on Rapid Prototyping*, Septembre, 14 – 15, 2004.

Tang, B.T.; Zhao, Z. & et al. (2007). Fast Thickness Prediction and Blank Design in Sheet Metal Forming Based on an Enhanced Inverse Analysis Method. *International Journal Mechanical Science*, Vol. 49, pp1018-1028, 2007.

Hu, S.; Li, Y.F. & et al. (2001) Modifying the shape of NURBS surfaces with geometric constraints. *Computer Aided Design*, Vol.33, pp903-912.

Batoz, J. L.; Guo, Y. Q. & Mercier, F. (1998) The inverse approach with simple triangular shell elements for large strain prediction of sheet metal forming parts. *Journal of Engineering Computation*, Vol. 15(7), pp864-92.

Lee, C. H. & Huh, H. (1998). Blank design and strain estimates for sheet metal forming processes by a finite element inverse approach with initial guess of linear deformation. *Journal of Materials Processing Technology*, Vol. 82(1-3), pp145-155.

Huang, Y.; Chen, Y. P. & Du, R. (2006). A new approach to solve key issues in multi-step inverse finite-element method in sheet metal stamping. *International Journal of Mechanical Sciences*, Vol. 48(6), pp591-600.

Lan, J.; Dong, X. H. & et al. (2005). Inverse finite element approach and its application in sheet metal forming. *Journal of Materials Processing Technology*, Vol.170 (3), pp624-631.

Reddy, J. N. & Reddy, J. (2007). *An Introduction to Finite Element Method*, McGraw-Hill, ISBN 9780071267618, New York, USA, 2005

Cui, Z. & Gao, L. (2010). Studies on hole-flanging process using multistage incremental forming. *CIRP Journal of Manufacturing Science and Technology*, Vol. 2(2), pp124-128.

IntechOpen



Rapid Prototyping Technology - Principles and Functional Requirements

Edited by Dr. M. Hoque

ISBN 978-953-307-970-7
Hard cover, 392 pages
Publisher InTech
Published online 26, September, 2011
Published in print edition September, 2011

Modern engineering often deals with customized design that requires easy, low-cost and rapid fabrication. Rapid prototyping (RP) is a popular technology that enables quick and easy fabrication of customized forms/objects directly from computer aided design (CAD) model. The needs for quick product development, decreased time to market, and highly customized and low quantity parts are driving the demand for RP technology. Today, RP technology also known as solid freeform fabrication (SFF) or desktop manufacturing (DM) or layer manufacturing (LM) is regarded as an efficient tool to bring the product concept into the product realization rapidly. Though all the RP technologies are additive they are still different from each other in the way of building layers and/or nature of building materials. This book delivers up-to-date information about RP technology focusing on the overview of the principles, functional requirements, design constraints etc. of specific technology.

How to reference

In order to correctly reference this scholarly work, feel free to copy and paste the following:

Yuanxin Luo, Kai He and Ruxu Du (2011). A New Rapid Prototyping Process for Sheet Metal Parts, Rapid Prototyping Technology - Principles and Functional Requirements, Dr. M. Hoque (Ed.), ISBN: 978-953-307-970-7, InTech, Available from: http://www.intechopen.com/books/rapid-prototyping-technology-principles-and-functional-requirements/a-new-rapid-prototyping-process-for-sheet-metal-parts

INTECH
open science | open minds

InTech Europe
University Campus STeP Ri
Slavka Krautzeka 83/A
51000 Rijeka, Croatia
Phone: +385 (51) 770 447
Fax: +385 (51) 686 166
www.intechopen.com

InTech China
Unit 405, Office Block, Hotel Equatorial Shanghai
No.65, Yan An Road (West), Shanghai, 200040, China
中国上海市延安西路65号上海国际贵都大饭店办公楼405单元
Phone: +86-21-62489820
Fax: +86-21-62489821

© 2011 The Author(s). Licensee IntechOpen. This chapter is distributed under the terms of the Creative Commons Attribution-NonCommercial-ShareAlike-3.0 License, which permits use, distribution and reproduction for non-commercial purposes, provided the original is properly cited and derivative works building on this content are distributed under the same license.

IntechOpen

IntechOpen